Evaluation of Ultrasonic vibration Assisted Grinding of Glass Using Photoelastic Method

Natsuki Sasada[1,a], Satohiro Yokoyama[1,b], Yuya Igarashi[1,c], Keisuke Hara[2,d] , and Hiromi Isobe[1,e]

[1]Department of Engineering, Nagaoka University of Technology
Kamitomioka 1603-1, Niigata, Japan
[2]Department of mechanical Engineering, National Institute of Technology, Ichinoseki College
Takanashi Hagisho, Ichinoseki, Iwate, Japan

[a]s153048@stn.nagaokaut.ac.jp, [b]s153089@stn.nagaokaut.ac.jp,
[c]s163007@stn.nagaokaut.ac.jp
[d]hara@ichinoseki.ac.jp, [e]isobe163@mech.nagaokaut.ac.jp

Key words: Difficult-to-cut material, Electro-deposited diamond wheel, Photoelasticity, Stress distribution, Ultrasonic machining

Abstract. Ultrasonic vibration of a grinding wheel is known to improve grinding processing properties such as suppression of wheel loading and reduction of grinding force. Especially for brittle materials such as glass and ceramics, many reports have described that ultrasonic vibration decreases crack generation and enhances productivity. Nevertheless, many questions persist about ultrasonic grinding mechanisms. Furthermore, a dynamometer, generally used to measure the grinding force quantitatively, is difficult to measure the dynamic phenomenon caused by ultrasonically vibrating abrasive grains. This study investigated glass grinding processes with visualization of stress distribution based on photoelastic method. The stress distribution on soda-lime glass caused by a 3-mm-diameter diamond electro-deposited wheel was visualized. Results distinguished clearly that the grading stress occurred individually below the grain. The phase difference image captured using a polariscopic was calibrated using an indentation test. Ultrasonic grinding reduced the instantaneous maximum grinding force to one-fifth.

1. Background.

Ultrasonic vibration of grinding wheel is known to improve grinding processing properties such as suppression of tool loading and reduction of grinding force [1, 2]. Improvement of processed surface properties has been reported for grinding hard brittle material such as glasses and ceramics [3]. However, the mechanism underlying these improvements has not been elucidated well. Traditional measure may not elucidate the effects of the ultrasonic vibration that is a dynamic process of machining. For example, a dynamometer, generally used to measure the total grinding force quantitatively, is difficult to detect the dynamic phenomenon caused by individual ultrasonically vibrating abrasive grain. The photoelastic method coupled with the high-speed camera is an established technology for visualizing the phase difference distribution change in the ultrasonic vibration band [4].

We applied the stress visualization method using photoelastic to monitor internal stress in soda-lime glass that was drilled using a diamond electro-deposited grinding wheel. Then we examined ultrasonic vibration effects on the stress distribution.

2. Experiment.

2.1 Experimental equipment and method.

Figure 1 presents an outline of the equipment we used for the ultrasonic-vibration-assisted grinding experiment. The spindle of the tool vibrated in the axial direction at 42 kHz (specification). Its amplitude was 4 μm (specification), the tool rotation speed was 5000 min^{-1}.

The feed rate of the tool was 0.4 mm/min, as shown in Table 1.

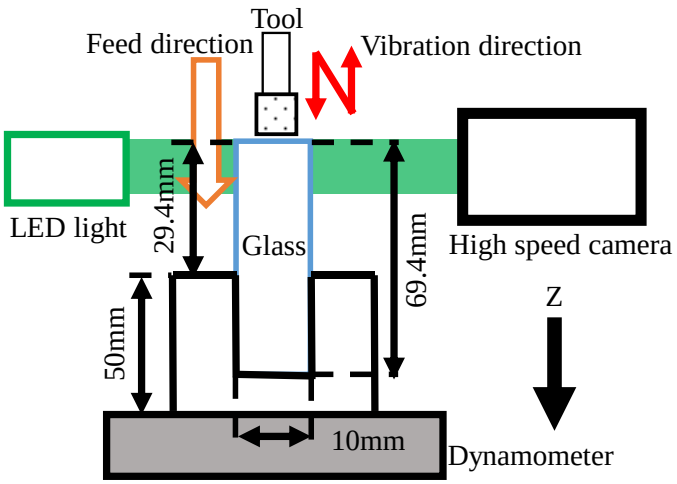

Figure 1 Experiment equipment.

Table 1 Experimental conditions

Feed rate	0.4[mm/min]
Rotation speed	5000 [min^{-1}]
Frequency of ultrasonic vibration	42 [kHz]
Amplitude of ultrasonic vibration	4 [μm]
Sampling frequency	20 [kHz]
Work	Soda-lime-glass
Coolant	Water

The tool was a 3.0-mm-diameter diamond electrodeposited grinding wheel. The grindstone grain size was #100. We selected a soda-lime glass piece for the work and used a tool dynamometer (Natural frequency: 5.6 kHz, spec.) with sampled data at a frequency of 20 kHz corresponding to 240 data acquisitions per tool rotation. Tap water is applied into the drilled hole as the grinding fluid. The ground area was filled by water tub in order to avoid the disturbance of optical path of photoelastic images due to water.

2.2 Visualization of phase difference distribution.

Dielectric media such as glass and acrylic resin show birefringence when an external force is applied. The photoelastic method makes use of a polariscope to observe the stress by detecting the phase difference of polarized light, showing birefringence caused by stress in photoelastic bodies [5]. For this study, we used a polarizing high-speed camera to shoot the polarized light penetrating glass being ground. The captured images of polarization information are processed to produce the phase difference image. In a plane stress condition, the principal stress difference is proportional to the phase difference by Brewster's law, the fundamental equation in the photoelastic method. The polarization camera shutter speed was set as 0.1 ms to generate 111 frames of phase difference images per tool revolution.

3. Effects of ultrasonic vibration on the grinding force.

We ground a 1.5 mm deep hole to ascertain the ultrasonic vibration effects. Grinding proceeded in the order of (a) Grinding with ultrasonic vibration assist (depth Z= 0–0.5 mm), (b) Grinding without assist (Z=0.5–1.0 mm), and (c) Grinding with assist (Z=1.0–1.5 mm). Consequently, (c) Grinding with assist (Z=1.0–1.5 mm) was done after (b) Grounding without assist (Z=0.5–1.0 mm) to verify the reproducibility of the ultrasonic vibration effects.

Figure 2 shows time variation of the grinding force. In (a), (b), and (c) of this figure, wide fluctuations of grinding force occurred every other second, resulting in large variations of stress as well. This variation might have been forced chattering vibration caused by glass work fixed on the jig. When comparing (a) and (c) of grinding with assist and (b) of grinding without assist, one might recognize a substantial reduction of stress fluctuation because of the ultrasonic vibration assist.

Figure 3 presents images of the phase difference distribution at the instant when the tool dynamometer recorded maxima for (a) Grinding with vibration assist (Z=0.5 mm), (b) Grinding without assist (Z=1.0 mm), and (c) Grinding with assist (Z=1.5 mm). These are all image-processed phase differences are depicted as hues that changes from phase difference of 0 nm (blue) to 66 nm (red). Below the tool shadow, one can recognize regions of large phase difference. In these regions, the abrasive diamond grains of the tool were pressed to the glass work surface. They ground that surface. The phase difference changed with rotation of the grains.

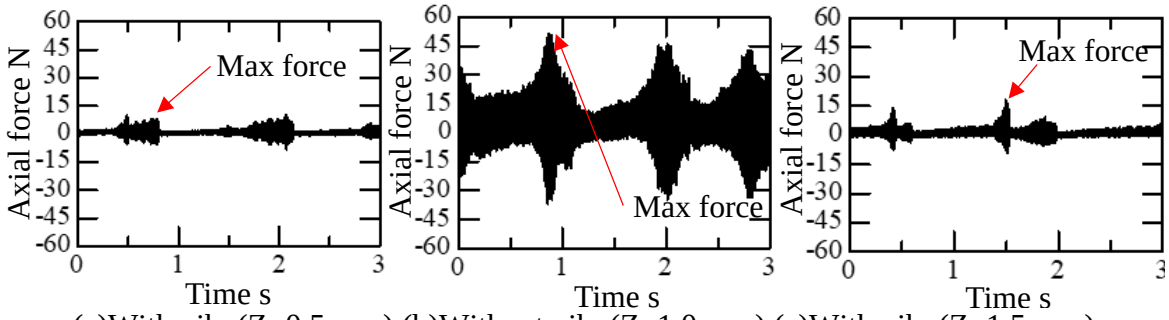

(a)With vib. (Z=0.5 mm) (b)Without vib. (Z=1.0 mm) (c)With vib. (Z=1.5 mm)

Figure 2 Time variation of the grinding force (Time [s] vs. Axial force [N]).

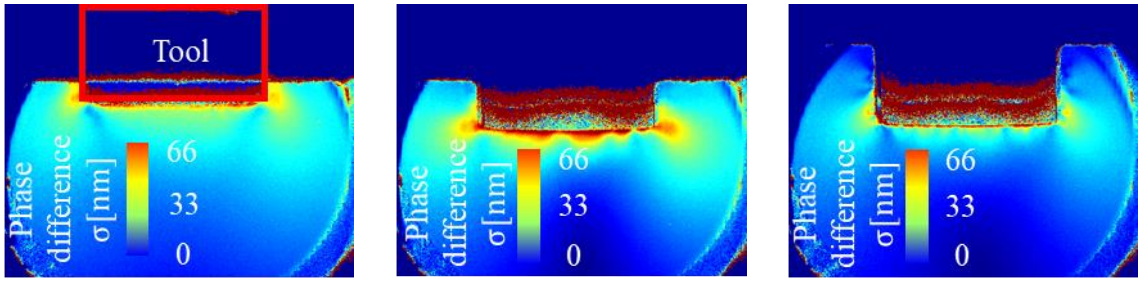

(a)With vib. (Z=0.5 mm) (b)Without vib. (Z=1.0 mm) (c)With vib. (Z=1.5 mm)

Figure 3 Image of phase difference distribution

We examined the time variation of the grinding force, as shown in Figure 2, and the image of phase difference distribution, Figure 3, to assess the reduction of grinding force by ultrasonic vibration assist. The maximum grinding force was 10.0 N for (a) Grinding with ultrasonic vibration assist (Z=0.5 mm) and 51.3 N for (b) Grinding without assist (Z=1.0 mm). From comparison of the phase difference distributions in Figure 3, one might find a smaller extent of the phase difference distribution for (a) Grinding with ultrasonic vibration assist (Z=0.5 mm) than that for (b) Grinding without assist (Z=1.0 mm). Generation of cracking and chipping in the grinding glass might be suppressed by reduction of the grinding force [6]. The maximum grinding force for (c) Grinding with assist (Z=1.5 mm) was 18.1 N. We recognized reduction of the maximum grinding force by ultrasonic vibration assist, again evaluating variation of the grinding force and the phase difference distribution.

Now, we discuss the reduction of grinding force by consulting the image of the phase difference distribution shown above. Phase differences caused by stress become visible immediately below the tool in (b) Grinding without assist. This phase difference might be generated by the grinding force pushing the tool down axially.

The extents of phase difference distribution in (a) Grinding with ultrasonic vibration assist (Z=0.5 mm) and (c) Grinding with assist (Z=1.5 mm) are smaller than that in (b) Grinding without assist. The intermittent grinding caused by the grinding grains' alternating collision

with the glass surface and separation from it in the frequency band of ultrasonic vibration suppressed the grinding force [7]. However, we were unable to learn the contribution of each grain to the phase difference distribution. Therefore, we conducted another grinding experiment with abrasive grains on a limited region of the bottom surface of the tool. The result is described in the next chapter.

4 Grinding by tools with limited working abrasive grains.

4.1 Experimental method.

Figure 4 depicts a photograph of the bottom surface of the tool used for this experiment. The abrasive grains worked were contained in a circle with about 1 mm diameter in the bottom surface of the tool. The circle center was 1.4 mm distant from the rotational center of the tool. All abrasive grains outside of this circle were removed by a diesinking electric discharge machine with a 1 mm inner diameter electrode. Consequently, using limited working abrasive grains, we were able to observe and discuss the actions of a few grains.

The average diameter of our # 100 abrasive grains was 160 μm. Six or seven grains were included in the circle described above. Hereinafter, we call this tool a tool with limited working abrasive grains. Making use of this tool, we conducted an experiment under the conditions shown in Table 2 and shot the polarized light image to get information about the phase difference distribution during grinding of soda-lime glass.

4.2 Experimental results.

Figure 5 portrays a phase difference distribution taken by shooting the image of polarized light for grinding using the tool with limited working abrasive grains at a feed rate of 1.0 mm/min. The photograph at the far left shows the phase difference distribution before the start of grinding. The other three were shot during grinding. The region of large phase difference indicated by the red arrow moved from right to left. The tool with limited working abrasive grains did grinding in the region with a wide phase difference distribution.

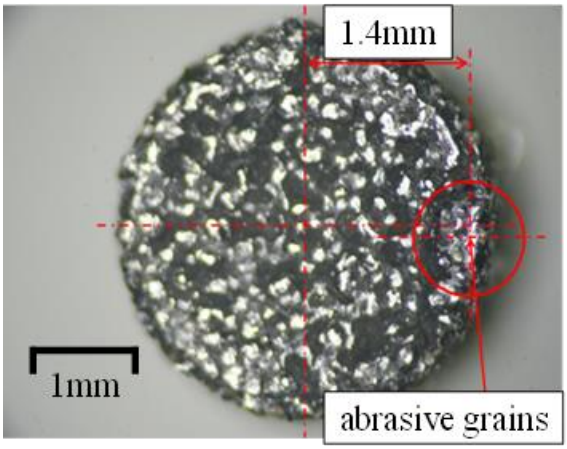

Figure 4 Tool with limited working abrasive grains.

Table.2 Experiment conditions

Rotation speed	5000 [rpm]
Feed rate	1.0 [mm/min]
Depth of cut	0.02 [mm]
Frame rate	9300 [fps]
Shutter speed	1/9300 [s]
Wavelength	530 [nm]
Pixels	1024×800 [pixel]
Work piece	Soda-lime glass (t = 8 [mm])
Grain size	#100
Diameter of tool	3.5 [mm]

Figure 6 presents the normal component of grinding force measured using the dynamometer. We defined the start of grinding as the instant when the grinding force on the work exceeded some threshold value. We set the time as 0.0 s there. The tool made one revolution in 12 ms; it was fed by 2 μm at the same time. The maximum grinding depth was found as 20 μm through examination of the grinding trace on the work. Therefore, the tool

arrived at the maximum depth in 1.2 s making 100 revolutions. Accordingly, the normal component of the grinding worked from 0.0 s to 1.2 s.

The red polygonal line in the figure shows the moving average of grinding force for one tool revolution. The force changed from one revolution to another. During the grinding work, we detected vibration of some 5 Hz and estimated that this vibration resulted from the brittle fracture of abrasive grains. Increase the grinding force for each 12–13 revolutions of the tool from the start of grinding and occurrence of the brittle fracture seen in the grinding trace in Figure 7 suggest that the tool ground the glass work by brittle fracture.

Figure 8 presents the phase difference distribution during 0.0–1.2 s of grinding by the tool. The abrasive grains were located immediately above the region with a wide phase difference distribution. The tool made 25 revolutions every 0.3 s.

Figure 9 depicts the difference of phase differences between that before grinding and those at 0.0, 0.3, 0.6, 0.9, and 1.2 s shown in Figure 8. Because the hue is shown in grades of 30 nm, we counted pixels between 10 nm and 30 nm and calculated the difference of pixels between them before grinding and those during grinding. From this graph, one might learn quantitatively the extent of the region with phase difference greater than 10 nm. This graph behaved like values of grinding force measured using the dynamometer, Figure 6.

5. Conclusion.

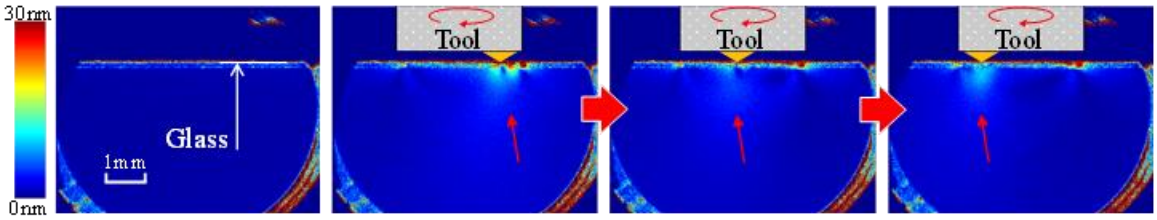

Figure 5 Phase difference caused by the tool with limited working abrasive grains.

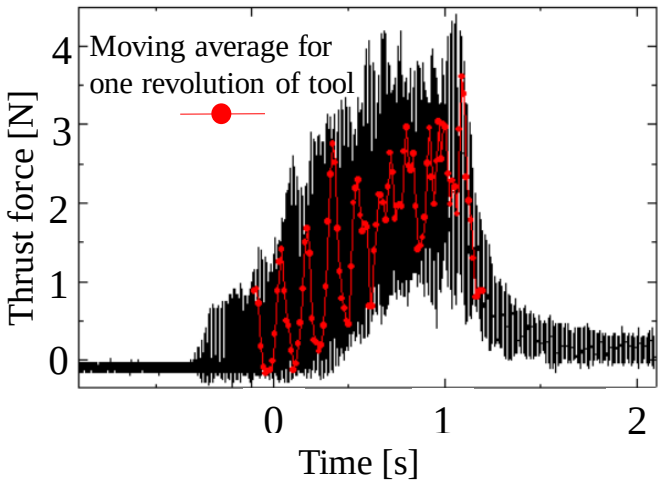

Figure 6 Grinding force by tool with limited working abrasive grains.

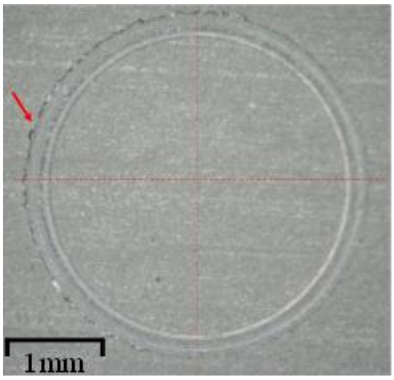

Figure 7 Machining marks by tool with limited working abrasive grains.

We executed two experiments of visualizing phase difference distribution using photoelastic method and grinding by tool with limited working abrasive grains, both in grinding work of soda-lime glass. The results can be summarized as presented below.

(1) Shooting the image of phase difference distribution caused by stress in glass piece being eing ground by photoelectric method, we were able to visualize the phase difference distribution

(2) Axial tool vibration of grinding tool reduced the maximum grinding force compared to that without vibration assist. From comparison of the extents of phase difference distribution, we found that those in (a) Grinding with ultrasonic vibration assist (Z=0.5 mm) and (c) Grinding with assist (Z=1.5 mm) were smaller than that in (b) Grinding without assist.

(3) (c) Grinding with assist (Z=1.5 mm) was done after (b) Grinding without assist (Z=1.0 mm), which showed again the reducing effect of ultrasonic vibration on the grinding force.

(4) Visualizing the image of phase difference distribution during grinding work by a tool with limited working abrasive grains, we learned how abrasive grains contributed to grinding. The phase difference distribution during this grinding work behaved similarly to the grinding force shown against the tool feed measured using the dynamometer.

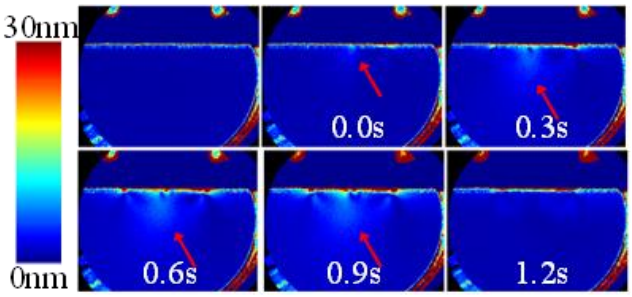

Figure 8 Phase difference during processing.

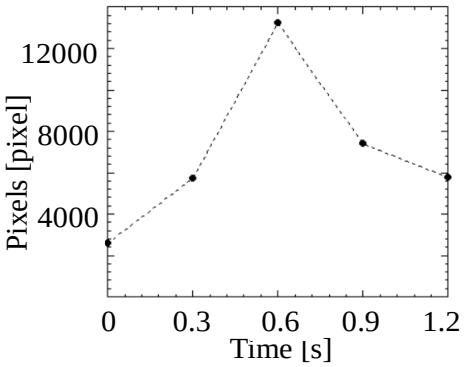

Figure 9 Difference of pixels between before and during grinding.

6. Acknowledgments

Photron Corporation provided us with valuable advice for which the authors are grateful. This study was financially supported by Grants-in-aid for Scientific Research 26289014.

7. References.

[1] T. Yamasaki, J. Yan, High precision drilling of CFRP by ultrasonic vibration-assisted grinding, JSAT. vol.59 no.12. (2015) 699-704.

[2] M. Nomura, Y. Wu, M. Kato, T. Tachibana, and T. Kuritagawa, Study of internal ultrasonic vibration assisted grinding of small bore - Mechanism of grinding force reduction due to ultrasonic vibration-, JSAT, vol.49 no.12. (2005) 691-696.

[3] J. Wang, K. Shimada, M. Mizutani and T. Kuriyagawa, Material Removal Mechanism in Micro Ultra Machining, Journal of JSPE. vol.82 no.5. (2016) 442-425

[4] H. Isobe, C. Yamaguchi, High-speed Capturing of Stress Distribution of Workpiece Under Ultrasonically Assisted Cuttung Condition, JSPE. vol.81 no.5. (2015) 441-445.

[5] E. Umezaki, Stress Distribution Measurement Techniques Using Photoelasticy : Current Status and Future Prospects, JSPE. vol.79 no.7. (2013) 607-611.

[6] A. Mizobuchi, H. Ogawa, and T. Sasaoka, Grinding force and crack size on through-hole drilling of glass plate used electroplated diamond tool in helical drilling, JSAT. vol.54 no.12. (2010) 731-736.

[7] H. Isobe, K. Hara, Technology of ultrasonic vibration assited machining -Basics of device design and application, Kagakuzyouhousyuppan, Japan, 2017.